


Enhancing Efficiency and Reliability of Electric Vehicles via Adaptive E-Gear Control

Conference Paper**Author(s):**

Sandel, Luca; [Zardini, Gioele](#) ; Mitrova, Sofija; Thekemuriyil, Tanya; Minamisawa, Renato; Rahimo, Munaf; Censi, Andrea; Frazzoli, Emilio; Mastellone, Silvia

Publication date:

2023

Permanent link:

<https://doi.org/10.3929/ethz-b-000626482>

Rights / license:

[In Copyright - Non-Commercial Use Permitted](#)

Originally published in:

<https://doi.org/10.1109/ITSC57777.2023.10421872>

Funding acknowledgement:

180545 - NCCR Automation (phase I) (SNF)

Enhancing Efficiency and Reliability of Electric Vehicles via Adaptive E-Gear Control

Luca Sandel¹, Gioele Zardini¹, Sofija Mitrova², Tanya Thekemuriyil², Renato Minamisawa², Munaf Rahimo³, Andrea Censi¹, Emilio Frazzoli¹, Silvia Mastellone²

Abstract—Battery Electric Vehicles (BEVs) offer a sustainable alternative to Internal Combustion Engine Vehicles (ICEVs). This paper addresses some of the challenges faced by the automotive industry and the scientific community in defining the technology for the next generation of automotive power converters. The focus is on achieving an improved drivetrain’s energy efficiency, enhancing drivetrain reliability, while minimizing costs to enable large-scale adoption of BEVs and Hybrid Electric Vehicles (HEVs).

The paper leverages an automotive converter equipped with the recently developed Adjustable Hybrid Switch (AHS) based electric gear and proposes a reliability-based control algorithm for operating the converter E-Gear (EG) of BEVs. By integrating reliability control principles, the proposed algorithm minimizes system damage over time and enhances the converter’s lifetime. The case studies, based on standardised driving cycles, demonstrate the benefits of the presented approach in terms of energy losses and lifetime expectations. Overall, this work contributes a novel approach to drivetrain control in BEVs, highlighting the potential of the proposed control strategy to improve energy efficiency and reliability. The research findings provide valuable insights for the development of next-generation automotive power converters.

I. INTRODUCTION

Battery Electric Vehicles (BEVs) hold the potential to provide a sustainable alternative to Internal Combustion Engine Vehicles (ICEVs). Currently, every major automotive manufacturer (e.g., Toyota, Mitsubishi, Ford, Renault, Nissan) is shifting to a full-electric lineup of vehicles. Together with the scientific and technical communities, they are faced with the challenge of shaping the technology for the next generation of automotive power converters. Typically, these are expected to perform with an abatement of CO₂ emissions (when considering tank-to-wheel performance), improved energy efficiency and reliability for a wide range of BEVs/Hybrid Electric Vehicles (HEVs), while maintaining a reduced cost, thus enabling the large scale adoption of BEVs [1]–[4]. Such issues are even more crucial when considering future Autonomous Mobility-on-Demands (AMoDs) services leveraging BEVs, due to the demanding computation (and energetic) needs of the autonomy stack [5], [6]. Addressing some of the described critical challenges is the focus of the present work.

¹Institute for Dynamic Systems and Control, ETH Zürich, Switzerland {lsandel, gzardini, acensi, efrazzoli}@ethz.ch.

²Institute of Electric Power Systems, Fachhochschule Nordwestschweiz, Windisch, Switzerland, {silvia.mastellone, sofija.mitrova, tanya.thekemuriyil, renato.minamisawa}@fhnw.ch

³MTAL AG, munaf.rahimo@mtal.ch

This work was supported by the Swiss National Science Foundation under NCCR Automation, grant agreement 51NF40.180545 and by the Swiss Federal Office of Energy SFOE.

In this paper, we consider an automotive converter equipped with an Adjustable Switch Hybrid Concept (AHS) based electric gear technology, presented in [7], and propose an automatic gear control strategy to increment the range and lifetime of BEVs by reducing converter losses and damages.

a) Background: Power electronic converters are at the core of a BEV drivetrain [8], [9], and they enable power conditioning and adaptation to driving requirements over a wide range of driving conditions [10]. However, after the battery pack, they have been widely identified as the component most likely to fail [11].

The performance of a power converter highly depends on the operating conditions of semiconductor devices, which vary across applications and electrical loads. More recently, converter switching devices based on wide-bandgap (WBG) materials, such as silicon carbide (SiC) or gallium nitride (GaN), are becoming more ubiquitous, replacing the classic silicon-based (Si) devices. Converters with WBG devices allow for more efficient and reliable transformation and control of electrical power, with reduced device size and weight [12], [13]. Their high cost, however, still represents a strong limitation to the wide deployment of BEV.

Recently, a new converter switching concept has been introduced in [7], [14]: the AHS is an extension of the Cross Switch (XS) Hybrid concept, originally comprising a fixed parallel arrangement of Silicon Insulated-Gate Bipolar Transistors (IGBTs) and unipolar SiC Metal–Oxide–Semiconductor Field-Effect Transistors (MOSFETs), hence relying on the different electrical characteristics of both devices. In the AHS, the Si-IGBT to the SiC-MOSFET ratio is dynamically adjusted through the gate units depending on the load conditions, resulting in a variable configuration of the converter. The AHS provides the drive-train with an Electronic Transmission System or Gear functionality and, with proper control, offers a great opportunity to benefit from each device characteristic in the different load conditions during drive cycles, and enhance the overall converter efficiency and reliability at a reduced cost [15], [16]. Furthermore, experimental results in [17]–[19] demonstrate a loss reduction in the XS and AHS configurations.

In this research, we design a control algorithm, to operate the converter E-Gears (EG) of an BEV at the best *efficiency* and *reliability* for each driving-cycle and operating conditions. Typically, reliability studies measure a system resistance to failure over time, estimate expected lifetime, and predict time-to-failure. This information is used to either design components to maximize their lifetime, or planning

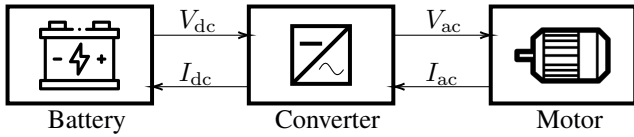


Fig. 1: BEV powertrain schematic, including a battery, a converter, and a motor, as well as the respective currents and voltages.

their maintenance or replacement. Operating a system for reliability, i.e., via reliability control, holds a great potential to minimize the damage of the system over time and improve its lifetime, and not much research work has been produced in this direction.

b) Statement of Contributions: Guided by the principles outlined so far, in this work we present a novel approach to the drivetrain control of BEVs of an AHS with EG. We design the online control strategy to *reduce* the converter losses and damage, and therefore *increase* its lifetime. The motor speed controller is modified adopting a gain scheduling strategy which computes at each instant of the drive cycle the best control policy based on the control target. The control policies are then tested on realistic case studies, where the speed profile of a real vehicle in a drive cycle is tracked by means of the presented control algorithm. The results are then compared with the a-posteriori evaluation of the drive cycle to assess the benefits in terms of energy losses and lifetime expectations. We illustrate how an online controller can be developed to improve particular drivetrain features.

c) Paper structure: This paper is structured as follows: Section II describes the automotive BEV power train and introduces the concept of AHS and EG. Section III details the semiconductor characteristics and its losses and damage models used to estimate the device efficiency and reliability. Section IV shows how we derive the control algorithms based on the provided estimates, and Section V presents the performance evaluation of the control strategy based on realistic case study simulations.

II. VEHICLE MODEL DESCRIPTION

The powertrain of a BEV is made of three main components: the battery pack, the DC/AC converter, and the electric motor (see Fig. 1). The power converter at the core of the powertrain converts the DC current supplied by the battery in the three-phase AC current necessary to drive the motor. It operates by means of transistors, which normally consist of silicon IGBTs. In recent years, this technology has been shifting toward WBG semiconductors, such as SiC-MOSFETs, which allow one to build equipment with smaller passive elements and smaller heat sinks, reducing the overall converter dimensions. Additionally, SiC-MOSFETs are characterized by lower switching losses across all operating ranges and conduction losses in subload regime, i.e., low voltage levels, as depicted in Fig. 2. SiC-based converters remain, however, one of the most expensive components in BEVs, and the one most likely to fail after the battery pack [11]. Hybrid solutions combining different types of devices in parallel have been proposed in [14], [17], [19], to

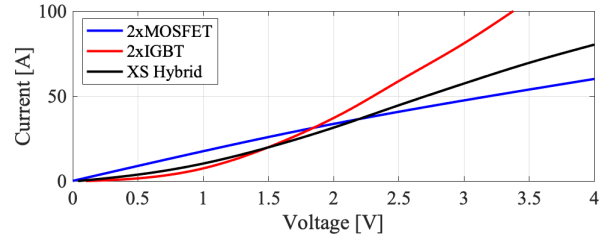


Fig. 2: IV characteristic of IGBTs, MOSFETs and XS hybrid semiconductors. The MOSFETs face lower internal resistances in the low load region compared to the IGBTs, leading to lower current losses. The behavior is reversed for the IGBTs, while the XS hybrid behaves like the average of the semiconductor coupling.

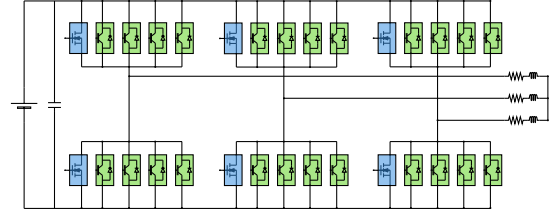


Fig. 3: Converter schematics. Each converter leg has four IGBTs and one MOSFET in parallel.

combine the properties of both devices obtaining an average efficiency (see Fig. 2).

In a further step, presented in [16], a new concept has been presented, where the parallel transistors in the XS hybrid are gate controlled separately, to select their optimal ratio based on power load, resulting in an electric gear. This solution combines the low conduction losses of MOSFETs in subload regimes with the low losses of IGBTs in high load regimes, resulting in an overall increase of the converter efficiency across all driving cycles and an overall cost reduction.

An example of the AHS converter configuration is depicted in Fig. 3, where the automotive converter is configured with a parallel combination of four IGBTs and one MOSFET. The SiC MOSFET alone is activated at the instants of low power of the drive profile, resulting in a first gear. The conditions for activating additional bipolar Si IGBTs depend on the operating load conditions. As such, the current is sensed in the output of the converter, and as soon as more current is required, more Si IGBTs will be activated sequentially, resulting in a higher gear level. The principle mimics conventional gears in an ICEV, where depending on the torque request expressed by the driver, a gear is selected to improve the vehicle's performance or fuel economy.

The device considered in this research operates with the gearing pattern observed in Fig. 4, where in first gear the current is sent across the MOSFET up to its peak efficiency current I_{MOS} , in second gear the first pair of IGBTs are coupled to the MOSFET, while in third gear all the semiconductors are activated. The current at which the gear switching happens has been determined offline according to the semiconductor properties and results from simulations, where it was evaluated that the highest efficiency could be achieved by switching at the semiconductor's peak efficiency current. This approach differs from what is described in [7].

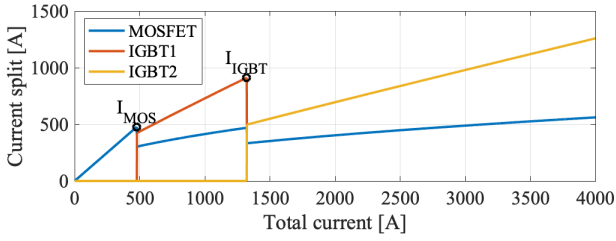


Fig. 4: Current split profile across the semiconductors in one converter leg. As the load current of the converter increases, more semiconductors are switched on, leading to the depicted current division.

Algorithm 1 Gear Selection

```

1: Input:  $I_{\text{mot}}, I_{\text{MOS}}, I_{\text{IGBT}}$ 
2: Output:  $G$ 
3: if  $I_{\text{mot}} \leq I_{\text{MOS}}$  then
4:   Engage Gear 1
5:    $G \leftarrow [1 \ 0 \ 0]$ 
6: else if  $I_{\text{mot}} > I_{\text{MOS}} \ \& \ I_{\text{mot}} \leq I_{\text{MOS}} + I_{\text{IGBT}}$  then
7:   Engage Gear 2
8:    $G \leftarrow [0 \ 1 \ 0]$ 
9: else
10:  Engage Gear 3
11:   $G \leftarrow [0 \ 1 \ 1]$ 
12: end if
13: Return  $G$ 

```

The gear is selected according to Algorithm 1, where G defines the output gear selected.

To leverage the potential of EGs in a BEV, we need to define a control strategy which selects instantaneous ratios of IGBT-MOSFET based on efficiency and reliability estimates in different load conditions. Thus, models for power losses and reliability for the semiconductors are required.

III. EFFICIENCY AND RELIABILITY MODELS

In the following, we consider both power losses and damage models for the individual devices, and derive behaviors for the whole converter.¹ Recall Fig. 2, which shows the linear characteristic of SiC-MOSFETs internal resistance versus the one of silicon IGBTs. Below the crossing point of the curves, for the same current level, the SiC-MOSFETs will require lower voltage due to its internal lower resistance which will produce lower conduction losses. When connecting multiple semiconductors of the same type in parallel, the current is evenly distributed among the active semiconductor components. In case of a hybrid configuration, the current is split among the transistors depending on the whole circuit voltage:

$$U_{\text{semi}} = \frac{\sqrt{V \cdot I_{\text{tot}} - W + X} - Y - Z}{2 \cdot a_{\text{IGBT}} \cdot n_{\text{IGBT}}}, \quad (1)$$

¹The semiconductor types considered are the Semikron IGBT SKM300GBD12T4 and the MOSFET SKM350MB120SCH15, connected in parallel according to a 4:1 ratio. The datasheets, describing the properties of both semiconductors can be found at [20], [21].

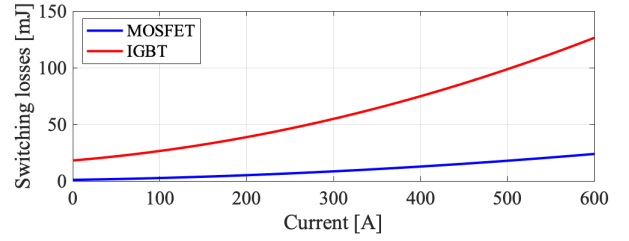


Fig. 5: Profile of the switching energy losses across the MOSFETs and the IGBTs. As the semiconductor current increases, the switching losses increment at a higher rate in the IGBTs compared to the MOSFETs

where:

$$\begin{aligned}
V &= 4 \cdot a_{\text{IGBT}} \cdot n_{\text{IGBT}}, \\
W &= (4 \cdot a_{\text{IGBT}} \cdot c_{\text{IGBT}} - b_{\text{IGBT}}) \cdot n_{\text{IGBT}}^2, \\
X &= 2 \cdot n_{\text{IGBT}} \cdot a_{\text{MOSFET}} \cdot b_{\text{IGBT}} \cdot n_{\text{MOSFET}}, \\
Y &= a_{\text{MOSFET}}^2 \cdot n_{\text{MOSFET}}^2 - a_{\text{MOSFET}} \cdot n_{\text{MOSFET}}, \\
Z &= b_{\text{IGBT}} \cdot n_{\text{IGBT}}.
\end{aligned} \quad (2)$$

The terms a , b and c for both IGBT and MOSFET can be typically found on manufacturer's data-sheets, and n_{IGBT} and n_{MOSFET} represent the number of active semiconductors. The current passing through each semiconductor is obtained as a function of the voltage:

$$I_{\text{IGBT}} = a_{\text{IGBT}} \cdot U_{\text{semi}}^2 + b_{\text{IGBT}} \cdot U_{\text{semi}} + c_{\text{IGBT}}, \quad (3)$$

$$I_{\text{diode}} = a_{\text{diode}} \cdot U_{\text{semi}}^2 + b_{\text{diode}} \cdot U_{\text{semi}} + c_{\text{diode}}, \quad (4)$$

$$I_{\text{MOSFET}} = a_{\text{MOSFET}} \cdot U_{\text{semi}}. \quad (5)$$

Once the individual semiconductor currents have been determined, the semiconductor losses are calculated by evaluating the conduction and switching losses. The former are the losses due to current transmission:

$$P_{c,z} = I_z \cdot U_{\text{semi}}, \quad (6)$$

where $z \in \{\text{IGBT}, \text{diode}, \text{MOSFET}\}$. The latter arise when the semiconductor is switched on, and re-calculated as a function of the switching frequency f_{sw} and the DC link voltage U_{DC} , considered in the parameter $\mu = f_{\text{sw}} \cdot U_{\text{DC}} / U_{\text{sw}}$:

$$P_{\text{sw},z} = \mu \cdot (a_{\text{sw},z} \cdot I_z^2 + b_{\text{sw},z} \cdot I_z + c_{\text{sw},z}). \quad (7)$$

The parameters $a_{\text{sw},z}$, $b_{\text{sw},z}$ and $c_{\text{sw},z}$ are obtained by the quadratic approximation of the energy switching characteristic of each semiconductor, typically provided by the manufacturer, and depicted in Fig. 5. The total losses of each semiconductor are calculated as the sum of conduction and switching losses, and are further evaluated to calculate the efficiency of the inverter during the drive cycle:

$$\eta_{\text{semi}} = \frac{P_{\text{out}}}{P_{\text{out}} + P_{\text{loss}}}. \quad (8)$$

Moreover, they are used to estimate the operational temperature of each semiconductor, which is calculated by means of the Foster model of the 5th order, as explained in [22].

The formula used to calculate the temperature at time-step k for each block is

$$T_{j,k,n} = T_{j,k-1,n} + (R_n \cdot P_{\text{loss}(k)} - T_{j,k-1,n}) \cdot (1 - e^{-\frac{t_s}{\tau_n}}), \quad (9)$$

where R_n is the resistance, t_n is the time constant and t_s is the sample time for the filter application. The values of these parameters vary depending on the type of semiconductor used, and can be found in [22], [23].

Finally, the damage accumulated in each semiconductor is calculated by analyzing the temperature profile by means of the Rainflow algorithm, presented in [24]–[26]. Practically, one extrapolates the local maxima and minima of the temperature profile, to investigate all the temperature ranges each semiconductor is subjected to during the drive cycle. The local extrema are then used to analyze the temperature cycles, from which the average cycle temperature T_{jm} and the delta cycle temperature $\Delta T_j = T_{j,\max} - T_{j,\min}$ are taken (in Kelvin). Then, T_{jm} and ΔT_j are used to compute the lifetime value N_f , coupled with terms from long time established power cycle models such as the technology coefficient A_0 , the Coffin-Manson exponent α , the activation energy E_a , the Boltzmann constant k_B and the time coefficient C and exponent γ , and terms depending on the semiconductor type, such as the time dependent scaling factor t_{on} and the thickness factor k_{thick} :

$$N_{fj} = A_0 \cdot \Delta T_j^\alpha \cdot e^{\frac{E_a}{k_B \cdot T_{jm}}} \cdot \frac{C + t_{on}^\gamma}{C + 2^\gamma} \cdot k_{\text{thick}} \quad (10)$$

Once the evaluation is carried for all temperature cycles, the overall damage D in the drive-cycle is then calculated as

$$D = \sum \frac{n_j}{N_{fj}}, \quad (11)$$

where n_j is the number of times the temperature cycle is repeated.

During operation, the MOSFET semiconductors maintain a more constant temperature compared to the IGBTs, due to their integrated reverse conducting diode, which result in lower cycle temperature swings (ΔT_j). This behavior makes the average temperature the primary damage source, in contrast with the IGBTs where temperature swings are higher, thus inducing higher damage. This, coupled with a low thickness factor, and higher average cycle temperatures, result in an overall reduced damage in subload regime.

IV. E-GEAR CONTROL FOR RELIABILITY AND EFFICIENCY

In this section, we consider a standard PI-based speed controller, designed to track a desired piece-wise constant motor shaft speed. This control strategy is chosen with autonomous systems in mind, as seen in [27], [28], where a controller is used to track the reference speed as opposed to a human driver generating a torque input via the accelerator pedal. The control variable is the electric torque that has to be generated by the power converter and will require a specific current.

The closed-loop dynamics for this system, that apply Newton's second law to the motor shaft, as seen in [29],

are:

$$\begin{aligned} \dot{\omega} &= \frac{\tau_e - \tau_l}{\Theta} \\ \tau_e &= k_p(\omega_{\text{ref}} - \omega) + k_I \int_{t_0}^{t_1} (\omega_{\text{ref}} - \omega) dt, \quad (12) \\ I_{\text{mot}} &= \frac{\tau_e}{K_{\text{mot}}}, \end{aligned}$$

where Θ is the moment of inertia of the motor, τ_l is the load torque applied to the shaft and τ_e is the motor torque, designed as a PI speed controller for speed tracking. The electric motor considered in the model is the emrax-188, and the input torque signal is saturated according to the motor capabilities expressed in the manufacturer's datasheet [30], where the maximum admissible torque is 100 Nm. From now on, we denote these (analog) dynamics as S_A . Furthermore, we refer to their discretized counterpart (computed, e.g., via Euler-forward discretization with a sampling time Δt) as S_D .

The mechanical power at the shaft is linked to the electrical power provided by the converter by means of Equation (12), where I_{mot} represents the motor phase current supplied by the DC/AC converter and τ_e is the torque input. The motor constant K_{mot} depends on the amount of pole pairs of the AC motor, the rotor inductance and the magnetizing inductance. The closed-loop system S_D is stable and achieves constant speed tracking for positive valued constant gains k_p and k_I . Those gains are typically designed to shape the system step response according to requirement specifications such as rise and settling time, and overshoot.

In order to leverage the additional degree of freedom during transient conditions, to achieve efficiency and reliability objectives, the gains can be adjusted online using a gain scheduling approach in [31]. With proper choice of the gains, the stability of the resulting closed-loop switched system under arbitrary switching conditions, can be shown via one common Lyapunov function [32].

Next, we characterize three cost functions, which contribute to the overall control objective, at each timestep i . To account for performance (i.e., the ability of our system to closely track the desired reference speed), the most aggressive PI gains have to be selected, therefore:

$$J_{\text{SPO},i} = -\| [k_{p,i} \quad k_{I,i}]^T \|^2. \quad (13)$$

Furthermore, to account for losses of our system (defined in Equation (6) and Equation (7)), we consider the cost

$$J_{\text{ECO},i} = P_{\text{loss},i}. \quad (14)$$

Finally, to account for damages (and hence reliability/lifetime of the components), we consider the cost

$$J_{\text{DAM},i} = [\alpha_i \quad \beta_{1,i} \quad \beta_{2,i}] \cdot G_i^T, \quad (15)$$

where G_i is found in Algorithm 1, and selects the semiconductors activated in each gear. The coefficients α, β_1, β_2 are a function of the semiconductor temperature T calculated in Equation (9), and are represented as

$$\begin{aligned} \alpha_i &= \sum_{j=0}^i \frac{T_{\text{MOSFET}}(t_j)}{i}, \quad (16) \\ \beta_{h,i} &= |(T_{\text{IGBT},h}(t_i) - T_{\text{IGBT},h}(t_{i-1}))|. \end{aligned}$$

By switching off the MOSFETs at higher current loads (i.e., high gears), the average temperature across the MOSFETs is kept lower, thus limiting the damage induced. For this reason, the gearing profile adopted in this paper varies to that described in Fig. 4, and the activation gear vector G is changed for gears 2 and 3 to $[0 \ 1 \ 0]$ and $[0 \ 1 \ 1]$, respectively.

In order to ensure closed loop speed stability and tracking, practitioners typically design k_p and k_I gains according to requirement specification. We will denote the set of gains corresponding to different step response requirements specification as K_p, K_I .

The motor torque command at each time-step is defined in Equation (12) and the gains are selected by solving the following optimization problem at each timestep:

$$\min_{K_p, K_I} w_1 \cdot J_{SPO} + w_2 \cdot J_{ECO} + w_3 \cdot J_{DAM} \quad (17)$$

s.t. System dynamics are given by S_D

Torque related to current according to Equation (12)

Gears are selected according to Algorithm 1,

The cost function weights $w_1, w_2, w_3 \in [0, 1]$ ($w_1 + w_2 + w_3 = 1$) are set to define the problem priorities and the driving style: eco, vs sport vs sustainable.

Given the pre-selected set of gains, the size of the problem allows one to perform exhaustive search to solve it online, and minimize the provided cost function, while satisfying the constraints. Extensions to this formulation are discussed in Section VI.

V. RESULTS

The control strategies developed in Section IV have been tested on the reference speed of the WLTP cycle simulated on an Aston Martin Cygnet. The WLTP cycle data is found on MATLAB/Simulink's Powertrain Blockset repository, the simulation is performed considering the vehicle dynamics outlined in [33], and the Aston Martin Cygnet data originates from [34]. The scenario is reproduced in MATLAB, where the reference is tracked with different control strategies. In particular, we look at case studies in which the cost functions are considered separately, focusing on tracking performance (referred to as SPO, $w_1 = 1, w_2 = w_3 = 0$), losses minimization (referred to as ECO, $w_2 = 1, w_1 = w_3 = 0$), and lifetime improvement/reliability (referred to as DAM, $w_3 = 1, w_1 = w_2 = 0$). The implemented strategies aim at selecting the best gain pairs, depending on the selected objective.

a) Performance mode (SPO): Intuitively, when in performance mode (SPO), the most aggressive PI values, which maintain the system stable, are selected at any given moment to reach the required top speed sooner. As seen in Fig. 6, the output speed tracks the reference motor speed closely, by implementing the most aggressive gains. This control performance is taken as the benchmark to calculate the controller losses and reliability of a standard, state-of-the-art, DC/AC converter, which operates to guarantee close reference tracking.

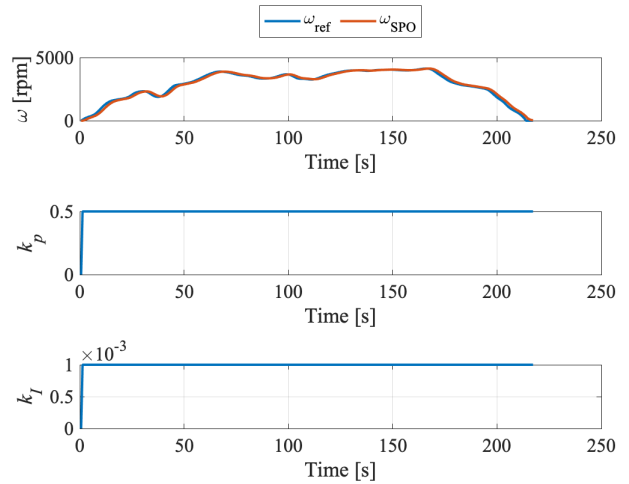


Fig. 6: Reference tracking and controller gains in SPO mode. The reference is tracked as closely as possible by taking the highest control gains available throughout the whole cycle.

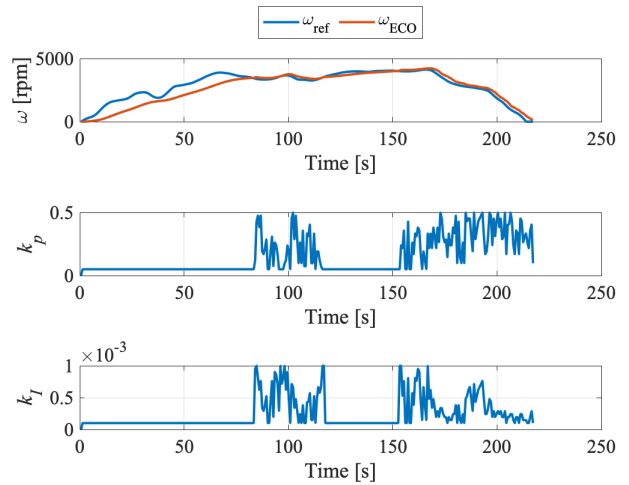


Fig. 7: Reference tracking and controller gains in ECO mode. At each instant the gain pair minimizing the losses is chosen as a function of the control error.

b) Losses minimization mode (ECO): When the system is controlled to allow for losses minimization (ECO), the control gains in the cycle change continuously to select the torque input implementing the gear with the lowest losses. As reported in Fig. 7, tracking performance is decreased, but the energy consumption is improved, thus allowing for battery range improvement and lowering the energy consumption during the cycle by 70% (i.e., from 91 Wh in sport to 14 Wh in ECO mode). Moreover, Fig. 8 shows how the power losses in ECO mode are kept at the lowest for most of the cycle. The occasional instances in which SPO and DAM modes show lower power losses take place because of the input power being lower in such instances.

c) Lifetime improvement mode (DAM): When controlling the system to improve lifetime, the aim is to keep the temperature of the IGBT constant, and the temperature of the MOSFETs low, since this induces the lowest damage to the

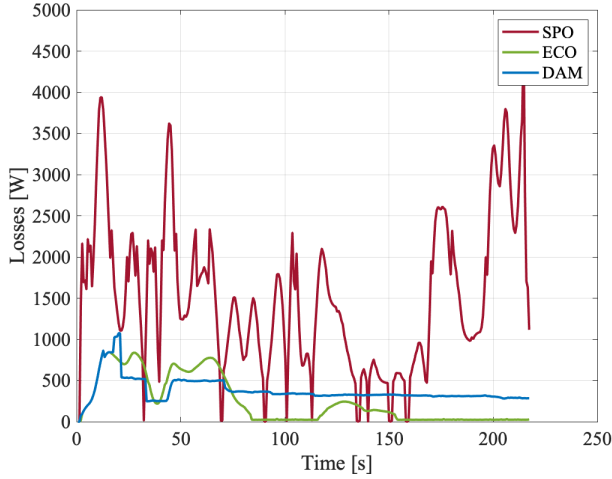


Fig. 8: Power losses comparison in SPO, ECO, and DAM modes. The losses in SPO mode are highest during most of the cycle, while the gain selection in ECO mode allows for the lower energy losses at the end of the cycle.

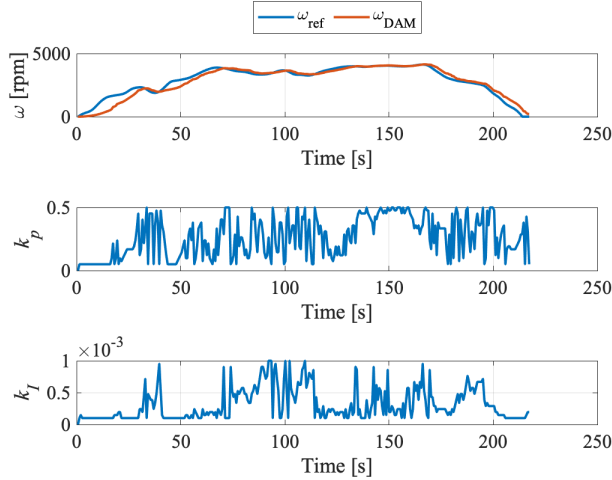


Fig. 9: Reference tracking and controller gains in DAM mode. The gains change continuously to achieve the desired temperature profile across the semiconductors, to induce the lowest damage.

semiconductors, as described in Section III and Section IV. This leads to the MOSFETs being very rarely switched on, as seen in Fig. 9. Thanks to this application, when evaluating the device lifetime with the Rainflow algorithm, an increase in converter lifetime is observed. Fig. 10 shows how, in reliability mode, only the IGBT1 module is switched on for most of the time, increasing the temperature of the IGBT2 module only when peak power is requested. This allows for the temperature of the IGBT1 to be kept as constant and as low as possible in order to achieve the highest lifetime score.

d) Comparison of modes: The results obtained with the different control modes are summarized in Fig. 11, where it is shown that sport mode achieves the lowest tracking error, while in ECO mode energy losses are reduced compared to SPO and DAM modes. Finally, when operating in DAM mode, the expected converter damage evaluated a-posteriori with the Rainflow algorithm in ECO and DAM modes sig-

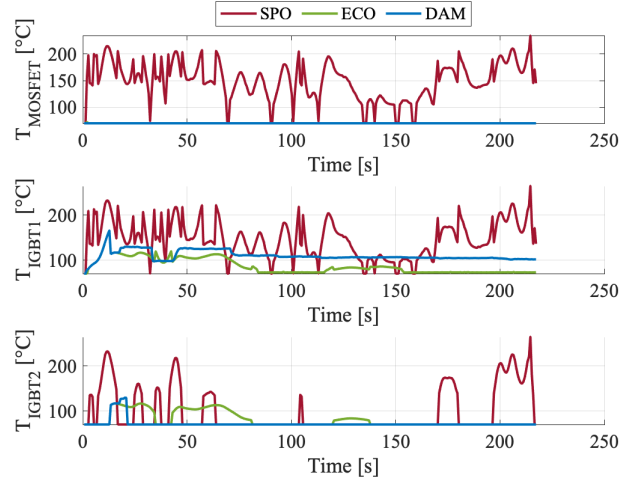


Fig. 10: Temperature profiles comparison in SPO, ECO, and DAM modes. In DAM mode the temperature of the IGBTs is kept constant for most of the cycle and the MOSFETs are kept switched off, as opposed to sport and performance modes that have higher and continuously changing temperature profiles.

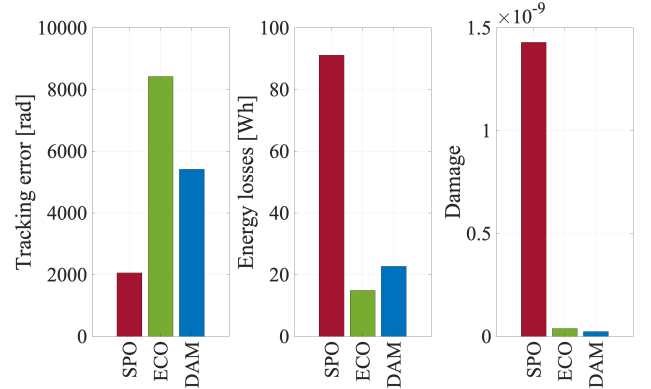


Fig. 11: Result comparison of different control modes. SPO mode achieves the lowest tracking error, ECO mode allows for the lowest energy losses during the cycle and DAM mode induces the lowest converter damage.

nificantly improves that achieved in SPO mode, decreasing the damage induced to the most stressed semiconductor by a factor of 100. These results show that by controlling the the DC/AC converter with an adequate control strategy, selected aspects of the BEV drive-train can be improved. In fact, simulations show that energy consumption can be reduced and the converter lifetime can be improved, thus increasing its reliability and the lifetime of the full drivetrain, making it less likely to fail.

VI. CONCLUSIONS

This paper shows how DC/AC converters can be operated to improve the performance, energy consumption and lifetime of BEVs. By means of a specific control strategy, EGs can be operated to reduce the converter's energy losses or reduce the damage induced by the temperature cycles, increasing its lifetime, which in turn improves the whole drivetrain's reliability. The operation of converters is characterized by a trade-off in the described quantities, and the

proposed methodology allows one to easily promote certain priorities, online, during the drive cycle.

The presented research unlocks exciting venues for future efforts. First, the proposed method can be enhanced by looking at how the developed control strategies interact with the design of the whole electric engine. In particular, this can be achieved by means of a mathematical theory of co-design, a methodology which has shown great applications in developing control strategies of future mobility solutions, all the way from the single platform, to the fleet level [35]–[37].

Second, we plan on extending the formulation presented in Section IV to a) leverage our knowledge about the system, and the influence of particular driving cycles on it, b) define a receding-horizon optimization problem, and c) solve it efficiently, by guaranteeing an optimal solution.

Finally, this research introduces the concept of control for reliability, which is an important, under explored, field of research. We plan on better modeling reliability of various components of BEVs, and including such models in the optimization of their operations.

REFERENCES

- [1] M. Fanoro, M. Božanić, and S. Sinha, “A Review of the Impact of Battery Degradation on Energy Management Systems with a Special Emphasis on Electric Vehicles,” 2022.
- [2] F. Spaven, Y. Liu, and M. Baghdadi, “Going further with smaller EVs: System-level battery range, emissions and charging infrastructure analysis,” *Journal of Cleaner Production*, vol. 369, 2022.
- [3] D. Pevec, J. Babic, A. Carvalho, Y. Ghiassi-Farrokhfal, W. Ketter, and V. Podobnik, “A survey-based assessment of how existing and potential electric vehicle owners perceive range anxiety,” *Journal of Cleaner Production*, vol. 276, 2020.
- [4] K. Sato, D. Navarro, S. Sekizaki, Y. Zoka, N. Yorino, H. J. Mattausch, and M. Miura-Mattausch, “Prediction of DC-AC converter efficiency degradation due to device aging using a compact MOSFET-aging model,” *IEICE Transactions on Electronics*, vol. E103.C, no. 3, pp. 119–126, 3 2020.
- [5] S. Sudhakar, V. Sze, and S. Karaman, “Data Centers on Wheels: Emissions From Computing Onboard Autonomous Vehicles,” *IEEE Micro*, vol. 43, no. 1, 2023.
- [6] G. Zardini, N. Lanzetti, M. Pavone, and E. Frazzoli, “Analysis and Control of Autonomous Mobility-on-Demand Systems,” *Annual Review of Control, Robotics, and Autonomous Systems*, vol. 5, no. 1, pp. 633–658, 6 2021. [Online]. Available: <https://www.annualreviews.org/doi/10.1146/annurev-control-042920-012811><http://arxiv.org/abs/2106.14827><http://dx.doi.org/10.1146/annurev-control-042920-012811>
- [7] M. Rahimo, R. A. Minamisawa, S. Mastellone, T. Koottungal, J. Spoendlin, T. B. Soeiro, and I. Nistor, “An advanced adjustable switch hybrid (Ash) concept for high power automotive converters,” in *PCIM Europe Conference Proceedings*, vol. 2021-May, 2021.
- [8] K. Sayed, A. Almutairi, N. Albagami, O. Alrumayh, A. G. Abo-Khalil, and H. Saleeb, “A Review of DC-AC Converters for Electric Vehicle Applications,” 2022.
- [9] S. Surya, S. P, and S. S. Williamson, “A Comprehensive Study on DC–DC and DC–AC Converters in Electric and Hybrid Electric Vehicles,” in *EAI/Springer Innovations in Communication and Computing*, 2022.
- [10] Phillip T. Krein, *Elements of Power Electronics*. Oxford University Press, 1 2015.
- [11] Q. Tang, X. Shu, G. Zhu, J. Wang, and H. Yang, “Reliability study of bev powertrain system and its components—a case study,” *Processes*, vol. 9, no. 5, 2021.
- [12] W. C. Alves, L. M. Morais, and P. C. Cortizo, “Design of an highly efficient AC-DC-AC three-phase converter using sic for ups applications,” *Electronics (Switzerland)*, vol. 7, no. 12, 2018.
- [13] A. Deshpande and F. Luo, “Comprehensive evaluation of a silicon-WBG hybrid switch,” in *ECCE 2016 - IEEE Energy Conversion Congress and Exposition, Proceedings*, 2016.
- [14] F. Kayser, F. Pfirsch, F. J. Niedernostheide, R. Baburske, and H. G. Eckel, “Novel Si-SiC hybrid switch and its design optimization path,” in *Proceedings of the International Symposium on Power Semiconductor Devices and ICs*, vol. 2022-May, 2022.
- [15] Y. Jiang, G. Hua, E. Yang, and F. C. Lee, “Soft-switching of IGBT’s with the help of MOSFET’s in bridge-type converters,” in *PESC Record - IEEE Annual Power Electronics Specialists Conference*. Publ by IEEE, 1993, pp. 151–157.
- [16] Y. Murakami, T. Takagi, K. Wada, and H. Matsunaga, “Essential structure of S-N curve: Prediction of fatigue life and fatigue limit of defective materials and nature of scatter,” *International Journal of Fatigue*, vol. 146, 2021.
- [17] U. R. Vemulapati, M. Rahimo, A. Mihaila, R. A. Minamisawa, C. Papadopoulos, and F. Canales, “The Bimode Cross Switch (BXS) a full hybrid solution in switch- and diode-modes,” in *2016 18th European Conference on Power Electronics and Applications, EPE 2016 ECCE Europe*, 2016.
- [18] M. Rahimo, F. Canales, R. A. Minamisawa, C. Papadopoulos, U. Vemulapati, A. Mihaila, S. Kicin, and U. Drofenik, “Characterization of a Silicon IGBT and Silicon Carbide MOSFET Cross-switch hybrid,” *IEEE Transactions on Power Electronics*, vol. 30, no. 9, 2015.
- [19] R. A. Minamisawa, U. Vemulapati, A. Mihaila, C. Papadopoulos, and M. Rahimo, “Current Sharing Behavior in Si IGBT and SiC MOSFET Cross-Switch Hybrid,” *IEEE Electron Device Letters*, vol. 37, no. 9, 2016.
- [20] “SEMISTRANS ® 3 GBD,” Tech. Rep. [Online]. Available: <https://www.semikron-danfoss.com/products/product-classes/igbt-modules/detail/skm300gbd12t4-22892212.html>
- [21] “SEMISTRANS ® 3 MB,” Tech. Rep. [Online]. Available: <https://www.semikron-danfoss.com/products/product-classes/sic/sic-mosfet/detail/skm350mb120sch15-21920190.html>
- [22] L. Siplika, B. Plassnegger, and M. Koller, “Junction temperature estimation for a high power sic traction inverter,” in *PCIM Europe Conference Proceedings*, vol. 2021-May, 2021.
- [23] Y. Zhu, M. Xiao, X. Su, K. Lu, Z. Wu, and G. Yang, “IGBT Junction Temperature Measurement under Active-Short-Circuit and Locked-Rotor Modes in New Energy Vehicles,” *IEEE Access*, vol. 8, 2020.
- [24] ASTM E1049, “Standard practices for cycle counting in fatigue analysis,” *ASTM Standard*, vol. 85, no. Reapproved 2017, pp. 1–10, 2017.
- [25] Z. Chen, F. Gao, C. Yang, T. Peng, L. Zhou, and C. Yang, “Converter Lifetime Modeling Based on Online Rainflow Counting Algorithm,” in *IEEE International Symposium on Industrial Electronics*, vol. 2019-June, 2019.
- [26] M. Musallam and C. M. Johnson, “An efficient implementation of the rainflow counting algorithm for life consumption estimation,” *IEEE Transactions on Reliability*, vol. 61, no. 4, 2012.
- [27] D. Turcian and V. Dolga, “Intelligent speed control system for electric vehicle,” in *IOP Conference Series: Materials Science and Engineering*, vol. 997, no. 1, 2020.
- [28] Z. Wang, G. Wu, and M. J. Barth, “A Review on Cooperative Adaptive Cruise Control (CACC) Systems: Architectures, Controls, and Applications,” in *IEEE Conference on Intelligent Transportation Systems, Proceedings, ITSC*, vol. 2018-November, 2018.
- [29] L. Guzzella and A. Sciarretta, *Vehicle propulsion systems: Introduction to modeling and optimization*, 2013, vol. 9783642359132.
- [30] EMRAX, “EMRAX 188 Technical Data.” [Online]. Available: <https://emrax.com/e-motors/emrax-188/#1482059435741-232ed37a-acc>
- [31] W. J. Rugh and J. S. Shamma, “Research on gain scheduling,” 2000.
- [32] D. Liberzon, *Switching in Systems and Control*, 2003.
- [33] G. Genta, *Motor vehicle dynamics - modelling and simulation*, 1996.
- [34] ultimatespecs, “Aston Martin Cygnet Specs.” [Online]. Available: <https://www.ultimatespecs.com/car-specs/Aston-Martin/24765/Aston-Martin-Cygnet-.html>
- [35] G. Zardini, Z. Suter, A. Censi, and E. Frazzoli, “Task-driven Modular Co-design of Vehicle Control Systems,” *Proceedings of the IEEE Conference on Decision and Control*, vol. 2022-Decem, no. Cdc, pp. 2196–2203, 2022.
- [36] G. Zardini, N. Lanzetti, A. Censi, E. Frazzoli, and M. Pavone, “Co-Design to Enable User-Friendly Tools to Assess the Impact of Future Mobility Solutions,” *IEEE Transactions on Network Science and Engineering*, vol. 10, no. 2, pp. 827–844, 2023.
- [37] G. Zardini, A. Censi, and E. Frazzoli, “Co-Design of Autonomous Systems: From Hardware Selection to Control Synthesis,” in *2021 European Control Conference, ECC 2021*, 2021.